Effect of Process Parameters on the Microstructure and Mechanical Properties of Bars from Al-Cu-Mg Alloy Processed by Multipass Radial-Shear Rolling

Torgom Akopyan
National University of Science and Technology
Yury Gamin
National University of Science and Technology
Sergey Galkin
National University of Science and Technology
Alexander Koshmin (koshmin.an@misis.ru)
NUST MISiS College of Environmentally Sound Technologies and Engineering https://orcid.org/0000-0002-4095-1658
Tatiana Kin
National University of Science and Technology
Vladimir Cheverikin
National University of Science and Technology
Alexander Aleshchenko
National University of Science and Technology

Research Article

Keywords: aluminum alloys, A2024 alloy, Al-Cu-Mg, radial-shear rolling, finite element simulation.

Posted Date: December 8th, 2021

DOI: https://doi.org/10.21203/rs.3.rs-1116468/v1

Abstract

The study of microstructure and mechanical properties formation of A2024 alloy obtained by the multipass radial-shear rolling (RSR) method is discussed in this article. FEM simulation was carried out that made it possible to evaluate the influence degree of rolling temperature-velocity parameters on the strain state of material. It has been found the increase in rotary velocity of rolls significantly influences on the deformation heating of bar after RSR (predominantly in its surface layer). The combination of rolling temperature-velocity conditions at selection of deformation regime has complex effect on structure and properties formation. The analysis of sizes and distribution of phase particles has shown that the rolling at lower temperatures allowed to increase the mechanical strength due to the more intensive refinement of undissolved Fe-containing phase. The gradual decrease in the rolling temperature in each pass makes possible to achieve the high strength (UTS~430 MPa and YS~255 MPa) while maintaining the ductility level ~15%, that are comparable to ones obtained at some severe plastic deformation (SPD) methods.

1. Introduction

The Al-Cu-Mg system alloys are basic materials for aerospace and automobile industries [1]. The alloy A2024 is a constructional material widely used for hulls and structural elements in mechanical engineering, aeronautics, and space where the minimum weight of structure plays a fundamental role [2, 3]. The semi-finished products in shape of bars are produced by method of hot extrusion mainly. The alloy is hardened by the quenching and subsequent natural or artificial aging [4].

During deformation in industrial conditions, the materials are exposed to the complex combination of strain, stress, and temperature changes. The understanding of metals and alloys deformation behavior during hot working is of a great importance, first of all, from the point of view of product properties formation. To study machinability and to establish optimal hot deformation parameters for certain metals and alloys, a number of research groups have made efforts to carry out thermomechanical experiments (compression, tensile and torsion tests) at wide temperatures and strain rates [5–8]. At the same time, the processes of metal forming in industrial conditions are different from the ones in laboratory. In particular, during the radial-shear rolling (RSR) the zonal temperature change and strain rate in wide range (from 0.1 to 100 s^{-1}) occur in depending on given rotary velocity of work rolls [9]. This fact indicates the need for research to find optimal deformation regime under conditions close to industrial ones.

Based on thermomechanical tests of samples for torsion, compression and tension, the different models of microstructure evolution during recrystallization have been constructed. The most famous models are McQueen [10], Hallberg [11, 12], Gourdet and Montheillet [13, 14], Sellars [15]. The most comprehensive review of dynamic recrystallization process in metallic materials was made by K. Huang and R.E. Logé [16]. One of the conclusions in this work is that there is a need to study the dynamic recrystallization mechanism under deformation conditions close to industrial ones since the microstructure evolution under these conditions is a more complex process than under constant ones. In addition, it depends on

deformation history and the initial state of the metal because industrial processes most often have several stages of deformation and heat treatment. In [17] the author made attempt to describe and to control the microstructure at dynamic recrystallization of steels during hot rolling. Based on the experimental data and revealed dependencies the processing maps were made which can be used to select the industrial rolling regimes and to build the rolling schedule. However, the results obtained also require confirmation by experimental studies in real conditions.

The radial-shear rolling method for obtaining the long bars with gradient functional structure in different materials is one of preferable due to its implementation simplicity and technological flexibility [18]. The equipment of RSR mills makes possible to obtain a wide range of product sizes and can provide different deformation degrees per pass [19]. The principle of this method and main distinctive parameters are described in detail earlier in publications of many authors [20–22].

The main purpose of this work is to determine the rational deformation regimes of aluminum alloy of system Al-Cu-Mg using RSR method from point of view of influence on microstructure and mechanical properties. To achieve this purpose, it is proposed to analyze the temperature conditions and deformation parameters at different rolling regimes using finite element method (FEM), as well as a study in laboratory conditions using industrial regimes.

2. Experimental Materials And Methods

2.1 Experimental procedure

Laboratory studies were carried out using radial-shear rolling mills “MISIS-100T” and “14-40”. These mills have the feed angle β and the toe angle δ equal to 20° and 10°, respectively. Work rolls are arranged symmetrically relative to rolling axis with a step 120°. Each work roll has the entrance angle on section of grip and reduction and the exit angle on calibration section. The special design of rolls and their geometrical arrangement ensure the movement of the workpiece along the helicoidally trajectory and, at the same time, its reduction along the diameter.

The cylindrical bar from industry alloy A2024 was used as an initial workpiece for rolling. Its chemical composition is presented in Table 1.

Table 1
Chemical composition of Al-Cu-Mg alloy, wt %

Al	Cu	Mg	Mn	Zn	Ti	Fe	Si	Ni
93.22	4.14	1.26	0.70	0.14	0.05	0.25	0.23	0.01

The diameter and length of initial workpiece were 60 mm and 130 mm, respectively. The initial workpieces were heated in batch-type furnace to rolling temperature T_0 for 2 h before deformation. The rolls were not additionally heated before deformation.

Temperature-velocity parameters of rolling are presented in Table 2.

Table 2
Temperature-velocity parameters of RSR

Regime number	Number of passes, Σi	Temperature, T_0 (°C)	Rolls rotary velocity, n (rpm)
1	5	450-400-350-300-250	30
2	5	450	30
3	30	450	30
4	5	300	90

In regimes 1, 2, and 4 the rolling was carried out to a final diameter of 14 mm in 5 passes (Ø60 - 42 - 31 - 24 - 17 - 14 mm) with varying the rolling temperature and rotation velocity of work rolls. The elongation ratio per pass μ_i is from 1.5 to 2.0 that makes it possible to avoid the significant deformation heating and to obtain the bar with an accurate geometric shape. The rolling with reduction along diameter of 2 mm per pass for regime 3 was carried out to determine the influence of large total number of deformation cycles on structure formation. After each pass, the bar was returned to the furnace to equalize the temperature across the section.

After rolling the part of samples was subjected to heat treatment (HT) according to regime shown in the diagram (Fig. 1).

2.2 Microstructure, phase composition and properties analysis

The microstructure was examined by scanning electron microscopy (SEM, TESCAN VEGA3) with an electron microprobe analysis system (EMPA, Oxford Instruments). The metallographic samples were ground with SiC abrasive paper, polished with 1 μm diamond suspension and etched with a 1% hydrogen fluoride (HF) water solution.

The phase composition of the alloy was assessed using Thermo-Calc software (TTAL6 database [23]).

The analysis of size and shape of secondary phases particles was carried out using the ImageJ (National Institute of Mental Health) program for images with a field size of 420x420 μm at a magnification of x500. To evaluate the shape of phases particles the shape parameter C (circularity) was calculated, it is determined by equation:

$$C = \pi \bullet \left(\frac{A}{P^2} \right) \quad (1)$$

where A is the area, mm^2; P is the perimeter, mm.

Circularity with a value of 1 indicates a perfect circle. As the value approaches 0, it indicates an increasingly elongated shape.

The cross-sectional microhardness of as-processed bar samples and heat-treated samples was measured by the Vickers method (HV) on a DUROLINE MH-6 installation (load 300 g, dwell time of 30 s) with the step of 0.5 mm from surface to center direction.

Room-temperature tension tests were conducted for as-processed bar samples and heat-treated sample with a universal testing machine, model Zwick Z250 (the loading rate was 10 mm/min). According to test results the ultimate tensile strength (UTS), yield strength (YS) and elongation to fracture (El) were obtained.

2.3 FEM simulation

The simulation of RSR process was performed using QFORM 3D (QuantorForm Ltd., Russia) program. For this, the solid 3D model consisting of rolls and workpieces was imported. The sizes and shapes of work rolls and workpieces correspond to the real ones at running of experiment. Temperature-velocity parameters of simulation are presented in Table 3.

Table 3
Temperature-velocity parameters of RSR in FE model

Regime number	Number of passes, Σi	Temperature, T_0 (°C)	Rolls rotary velocity, n (rpm)
1	5	450-350-300-250-200	30
2	5	450	30
3	5	400	30
4	5	350	30
5	5	300	90

The regimes 1, 2, and 5 correspond to the experimental ones of rolling. The regimes 3 and 4 were selected for a more comprehensive analysis of effect of heating temperature on deformation parameters.

After completion of calculation of each pass the bar temperature was set uniform along section again that corresponds to conditions of real experiment. Other workpiece parameters were saved and imported to the next operation.

The calculation was carried out considering the heat exchange between the workpiece and tool and the environment. The main parameters were set for model: rolls temperature – 25°C; ambient temperature – 25°C; coefficient of heat transfer between the material and the tool – 30000 W/m^2·K; coefficient of heat transfer between the material and the air – 30 W/m^2·K; friction factor – 0.93; rolls material – 40Cr steel.

The chemical composition, physical, mechanical, and rheological properties of A2024 commercial aluminum alloy can be found in QFORM database. The rheological properties of material are given as a table function for temperatures 250, 330, 400, 470 and 550°C, strain rates 0.01, 0.1, 1.0, 10, 50, 200 s^{-1}, and deformation degree from 0.01 to 0.99.

According to the calculation results, the parameters of the equivalent deformation ε over the cross-section of bar, the temperature distribution in deformation zone and after rolling were analyzed.

To determine the equivalent strain the numerical integration of strain rate intensity for each mesh node of workpiece among the movement trajectory of element particle of deformed metal is used in QFORM program:

$$\epsilon = \sum_n \dot{\epsilon}^n \Delta t_n, \quad (2)$$

where Δt_n is the time step of calculation; n is number of time step of calculation.

3. Results And Discussion

3.1 FEM modeling

3.1.1 Temperature analysis

At different velocity and temperatures of rolling the temperature changes of bar immediately in deformation zone is of interest to study. As shown in [9] these changes can lead to different combination of structure over bar cross-section during dynamic recrystallization. In this case, the temperature was controlled at three points: *P1* - bar center; *P2* - half of bar radius; *P3* - bar surface. The graphs of temperature changes at points *P1-P3* obtained by tracing of points along their movement trajectory are presented in Fig. 2. It makes possible to see the dynamic of temperature changes in zones typical for RSR.

As can be seen, the greatest temperature fluctuations (the change reaches 20-50°C per deformation cycle) occur in the surface layer of bar where strains and stresses are localized. Since the deformation zone is open, the sharp change in temperature in contact zone occurs with each single reduction by roll. In the moment of point *P3* passing between work rolls (non-contact area of deformation) the surface temperature can sharply change again.

At maximum heating temperature T_0 = 450°C the surface temperature in the deformation zone decreases while the temperature at points *P1* and *P2* smoothly increases in the reduction zone. At decrease in heating temperature of workpiece to 350-400°C the tendency to decrease in surface temperature of bar reduces, and the temperature at point varies in temperature range of *P1* and *P2*. (Fig. 2b, c). In the calibration zone of bar in all three cases the temperature fluctuations of surface reduce since the reductions are insignificant, and the temperature of inner layers almost do not change.

The rolling velocity also significantly impacts on the changes in temperature field of workpiece in the deformation zone. At the rotary velocity of 90 rpm the surface temperature in reduction zone intensively increases, the graph is stepped. (Fig. 2d). Since the time of one cycle decreases the temperature in the contact zone with colder roll have no time to change and remain the constant. It should be noticed in this case that the temperature gradient over section of bar ΔT sharply increases with the growth of rolling velocity. Difference between temperatures at points *P1* and *P3* is more 100°C, it can additionally effect on structure formation processes.

Since the rolling in an industry is mostly done in several passes, it is effectually to analyze the temperature change after each pass. The graphs of temperature change of bar after each pass ΔT relatively heating temperature before rolling T_0 for five simulated regimes are presented in Fig. 3. The change in temperature ΔT was determined as the difference between T_0 and average temperature at points *P1-P3* on the exit of deformation zone.

For regimes 2, 3, and 4 with constant temperature before each pass and the same rolling velocity it should be noticed that ΔT decreases with reducing of bar diameter. For higher heating temperatures of 400 and 450°C, the temperature increase is 50-70°C in the first pass, and there is no increase in the last one. For regime 1 with gradual decrease in temperature the deformation heating with each subsequent pass, on the contrary, increases. For the first pass, it is minimal and equals 25°C, and in the last pass it reaches approximately 100°C.

At the heating temperature 300°C and the increase in rotary velocity to 90 rpm the temperature increase after RSR is the largest and it is 90-125°C, for first four passes, and it decreases to 60°C in last pass.

Based on data obtained the following general conclusions can be made:

- at the same heating temperature before rolling T_0 the deformation heating of bars decreases with reduction of bar diameter;

- reducing the heating temperature by 50°C leads to a decrease in deformation heating by approximately the same amount;

- increase in the rotary velocity of rolls has a significant effect on the deformation heating of bar after RSR (mainly in surface layer of bar).

As can be seen, the combination of rolling temperature-velocity conditions at selection of deformation regime has complex effect that cannot be easily predicted or calculated analytically. Since the temperature is one of the main parameters effected on structure and properties formation the simulation can be useful tool for preliminary analysis and forecasting of product properties formation.

3.1.2 Deformation parameters analysis

The equivalent strain parameter can be used for the complex characteristic of technological process conditions influence on material properties. During the severe plastic deformation processes the large values of equivalent strain (4-6 or more) are achieved with relatively small changes in the overall dimensions of workpiece. It makes possible to obtain the materials with ultrafine-grain or nanostructure and significantly increase the strength properties. [24, 25].

During RSR process the field of equivalent strain is formed with pronounced gradient of distribution over section of rolled product. The equivalent strain ε reaches the maximum values in peripheral zone of workpiece where the greatest shear strains occur locally. The values of ε are minimal in the central zone and, mainly, determined by reducing of cross-section area of bar.

The temperature and rotary velocity of rolls significantly effect on the gradient of equivalent strain field. With decrease in the initial temperature and increase in the rotary velocity of rolls the growth of maximum values of ε at insignificant change in level of minimum values in the center is observed. In these dependencies the influence of rheological component on the strain state of workpiece is appeared. As known the deformation heating is due to dissipation of plastic deformation power which is proportional to flow stress and strain rate. Disregarding some conventions, it can be argued that the following self-activating scheme is implemented. The initial nonuniform distribution of ε creates nonuniform deformation heating. In the most heated near surface layers, the resistance to deformation of metal (flow stress) decreases, which contributes to an even greater localization of the accumulated strain on these layers with an increase in its maximum values. This, in turn, further enhances the deformation-temperature gradient. It is obvious that when implementing such scheme, the force of metal on roll decreases due to a decrease in the level of contact stresses during local heating. Data obtained at simulation (Fig. 4) appear this fact. For all studied regimes the growth of maximum values of ε and the increase in the gradient with the decrease in the rolling force are observed.

For a comparative analysis the development of severe plastic deformation area (SPD area) expressed in relative fraction of bar cross-section area with the value $\varepsilon \geq 8$ was determined for each regime (Fig. 5).

The greatest values of SPD area were recorded for regime 1 with gradual decrease in rolling temperature (83.86%) and regime 5 (82.30%). The decrease in deformation temperature from 450 to 400 °C leads to increase to SPD area by 4.5%. While the decrease in temperature to 350 °C increases this value almost by 14%. In the central zone of bar occupied approximately 1/3 of the radius, where the effect of strain rate

intensity is minimal [26, 27], the equivalent strain parameter is mainly determined by elongation in a given section (by reducing its area).

From the data obtained, it can be assumed that regimes 1 and 5 can have the greatest influence on properties and microstructure. The SPD area defined in this case by parameter of equivalent deformation ($\varepsilon \geq 8$) is localized in bar surface layer and depends not only on the magnitude of shear strain but also on the temperature-velocity regimes of processing.

3.2 Microstructure characterization and phase analysis

The microstructures of the as-processed (RSR) and heat treated (RSR+HT) bars obtained at different regimes (see Table 2) are presented in Fig. 6. Table 4 represents the quantitative data on the number, shape, and size of particles observed in the microstructures. For ease of reading, the latter data is also presented as histograms in Fig. 7. As can be seen that heat treatment leads to substantial decrease in the number density of particles observed in the as-processed structures. It may be deduced that the decrease in the number density after heat treatment is associated with dissolution of the fine Cu and Mg precipitates (represented by the Al_2Cu and Al_2CuMg phases) formed during the cooling of bars from the RSR temperature. As can be seen from Fig. 4, the fraction of the precipitates depends on the RSR temperature. Indeed, the higher fraction of precipitates can be observed for the samples obtained at low RSR temperature (regimes 1 and 4). The latter is due to the natural decrease of the Cu and Mg solubility with the temperature decrease. The coarser particles also observed in the structures are insoluble and belong to the Fe-containing phase. According to the thermodynamic calculation made using Thermo-Calc program, this Fe-containing phase should belong to the α(AlFeSiMn) compound [28].

Table 4
Data on size, number, and shape of phase particles in A2024 alloy

Regime Number		Center				Surface			
		Counts	Area %	Avg Size, μm	Circularity, *C*	Counts	Area %	Avg Size, μm	Circularity, *C*
1	RSR	20946	9.77	0.81	0.95	20680	11.93	0.99	0.93
	RSR+HT	1506	2.28	2.53	0.93	2770	1.93	1.21	0.96
2	RSR	9727	5.73	1.02	0.97	10188	6.32	1.07	0.96
	RSR+HT	829	1.48	3.08	0.91	1030	1.38	2.33	0.93
3	RSR	14447	6.91	0.83	0.97	11174	6.71	1.04	0.97
	RSR+HT	864	2.01	4.01	0.90	1219	1.17	2.79	0.93
4	RSR	19197	9.22	0.83	0.95	20157	9.72	0.83	0.95
	RSR+HT	3178	2.80	1.52	0.95	2025	1.74	1.49	0.95

The quantitative analysis (Table 4 and Fig. 7) well illustrates that after heat treatment the fraction of particles decreases to 2% area for all samples. These particles correspond to the undissolved Fe-containing phase, the fraction of which depends only on the concentration of Fe in the alloy. The linear size of these particles varies in the range of 1.5-4.0 μm and strongly influenced by the RSR regime. Indeed, for the regimes 1 and 4 characterized by the lowest processing temperature range from 250-350°C, the size of particles is smallest. For the bars processed at 450°C, the average linear size of the Fe-containing particles increases about two times. The obtained data on the influence of processing temperature on the particle liner size are in good agreement with the numerical simulation data on the influence of processing temperature on the equivalent strain (Fig. 5). The obtained data suggests development of much higher SPD area for the bars processed at low temperature regimes 1 and 4. The latter should lead to a more intensive refinement of the structure. It should be noted that the size of particles near the surface is noticeably less for most regimes except 4. The observed difference in particle size over the cross-section of workpiece is due to the natural gradient distribution of strains and stresses at RSR. Indeed, according to the previous studies [29, 30], higher strains and stresses are observed near the surface of workpiece. For the regime 4 the about equivalent size of the particles over the cross-section of workpiece can be observed. The latter result is due to the increased fraction of SPD area coupled with the highest equivalent strain which allows to process the workpiece more intensively through entire cross-section. In addition, from Fig. 7d it can be also observed that the morphology of all particles slightly depends on the processing regimes and most particles strongly tends to acquire a spherical morphology. It should be noted that the size and shape of undissolved Fe-containing particles strongly influence on the alloy mechanical properties (especially for ductility), and fine structure coupled with the spherical

morphology of the particles is most desirable one since it minimizes the detrimental influence of Fe-containing phase on the mechanical properties.

The grain structure of the 14 mm bar obtained at regime 1 was analyzed using EBSD in the near surface area and central area after both processing and processing and followed by high temperature annealing (~ 495°C for 1 h) before quenching. Color reveals the crystallographic orientation in the unit triangle of the standard stereographic projection. EBSD grain orientation maps of the longitudinal structure of the 14 mm bars are shown in Fig. 8 and 9. In the EBSD micrographs, black lines denote high angle boundaries (HAGBs) with misorientations greater than 15°, and grey lines are used to identify low angle boundaries (LAGBs) with misorientations between 2° and 15°. As can be seen from Fig. 8a, the structure in the near surface area is mainly deformed and characterized by the formation of fibrous grains elongated in the rolling direction. It should be noted that according to the numerical simulation the equivalent strain in this area reaches more than 20 (Fig. 4) which should be enough to trigger the dynamic recrystallization. However, the continuous decrease in the deformation temperature down to 250°C obviously hinders this process and formation of extensive net of LAGB can be instead observed. It should be also note that according to Fig. 3, the deformation heating during the last passes should be more than 100°C. However, due to the relatively small radius of the final bar and the contact with the cold rolls, most of this heat is dissipated and the resulting temperature is insufficient to activate recrystallization. Taking into account the size of sub-grains formed, the average grain size in this area is about 4 μm. Due to the increased strain energy stored during deformation, the annealing at 495°C for 1 h leads to intensive development of recrystallization (Fig. 8b and d) result in the substantial increase in the grain size and reduction in LAGB.

Similar studies for the central parts of the same bar revealed that after RSR the recrystallization also does not take place (Fig. 9c). The latter is due to the insufficiently high equivalent strain. Indeed, according to Fig. 5, the maximum equivalent strain in the central part reaches 6-8, which is more than two times less than for the surface. Result in the latter, the intensive formation of substructure and the grain size refined down to 8 μm can be observed. The much lower storage strain energy in this part prevents intensive recrystallization during high-temperature heating and thus the structure remains largely unrecrystallized, although the average grain size increases significantly due to an extent decrease in LAGB.

Thus, from the presented analysis, it can be observed that the deformation with a gradual decrease in temperature to 250°C leads to formation of the intensely deformed grain structure with an extensive net of LAGB. On the contrary, solid solution heat treatment activates recovery processes including recrystallization result in the formation of much coarse grain structure.

3.3 Mechanical properties

The graphs of microhardness distribution in cross-section of 14 mm bars obtained at different RSR regimes are presented in Fig. 11. The analysis showed the microhardness of as-processed bars is higher for lower processing temperatures (regimes 1 and 4). The latter is due to the more intensive strain hardening. An increase in the deformation temperature up to 450°C leads to a gradual decrease in

hardness (Fig. 10a) due to the development of recovery processes. The distribution of microhardness in cross-section of bars obtained at constant initial processing temperature (regimes 2, 3 and 4) is quit uniform. In case of bars obtained at 450°C, the increased processing temperature neutralizes the difference in equivalent strain between surface and center due to the intensive development of recovery processes toward the surface. For the bar obtained at low temperature 300°C and highest rotary velocity 90 rpm numerical simulation suggests highest difference in equivalent strain between surface and center (28 vs 8). However, the deformation heating, especially for near-surface regions, should also be maximum for this regime (Fig. 2d). Indeed, the temperature in the near surface area can reach 470°C which is even higher than that for the bars obtained at regimes 2 and 3. Thus, the high temperature similarly compensates for the high difference between the equivalent strain over the section of bar. Slightly higher hardness in the center of bar obtained at regime 1 can be explained by the higher temperature (due to the deformation heating at last passes) result in the increased solubility of Mg and Cu in aluminum solid solution.

The bars in the as-processed state were subjected to uniaxial tensile tests (Fig. 10b). The analysis revealed that the ductility for all samples is not less than 10%. Moreover, the bars obtained at low temperature regimes 1 and 4 have a higher ductility up to 15%. The latter result seems is due to the more intensive refinement of undissolved Fe-containing phase at low temperature processing. An increase in the processing temperature to 450°C provides low strength of the as-processed bar. Indeed, for the regime 2 UTS~285 MPa and YS~178 MPa. On the contrary, a gradual decrease in the processing temperature to 250°C (regime 1) led to significant strengthening. The strength properties of the as-processed bar obtained at regime 1 UTS~430 MPa and YS~255 MPa are close to ones usually obtained for this alloy after a full cycle of heat treatment, including quenching and aging. Thus, after processing the bar obtained at regime 1 has simultaneously highest strength and ductility which are comparable to ones obtained at different SPD methods [31, 32]. However, unlike the latter, RSR method used to obtain the bars can be applied in mass industrial production.

4. Conclusion

The analysis of temperature-velocity regimes of deformation for the A2024 aluminum alloy obtained by RSR method was discussed in this article.

1. All other conditions being equal, the decrease in heating temperature before rolling promotes to reducing of surface temperature fluctuations in deformation zone and to a more intensive deformation heating of bar during deformation. The increase in rotary velocity of rolls leads to a sharp growth of temperature gradient over bar cross-section.

2. The analysis of changes in temperature after RSR for different regimes shown that the deformation heating of bar decreased at equal heating temperature before rolling with a decrease in bar diameter. The decrease in temperature by 50°C leads to the reduction of deformation heating approximately by the

same value. The increase in rotary velocity of rolls significantly influences on the deformation heating of bar after RSR (predominantly in surface layer of bar).

3. Analysis of the microstructure of bars obtained at different regimes revealed that the linear size of the excess phases (primarily Fe containing) varies in the range of 1.5-4.0 μm and strongly influenced by the RSR regime. The size of particles near the surface is noticeably less, it is due to the natural gradient distribution of strain and stresses across the cross-section of bars obtained at RSR. Most particles strongly tend to acquire a spherical morphology. The size and shape of the undissolved Fe-containing particles strongly influence on the alloy mechanical properties (especially for ductility), and fine structure coupled with the spherical morphology of particles obtained at RSR is most desirable one since it minimizes the detrimental influence of Fe-containing phase on the mechanical properties.

4. The grain structure of the 14 mm bar obtained at regime with a gradual decrease in the deformation temperature from 450 to 250°C was analyzed using EBSD in the near surface area and central part after both processing and processing and followed by heat treatment. Analysis showed that the deformation with a gradual decrease in temperature to 250°C leads to formation of intensely deformed grain structure with an extensive net of LAGB. On the contrary, the solid solution heat treatment activates recovery processes including recrystallization result in the formation of much coarser grain structure.

5. The bars in the as-processed state were subjected to uniaxial tensile tests. The analysis revealed that an increase in the processing temperature to 450°C provides lower strength (UTS~285 MPa and YS~178 MPa) and ductility (~11%). On the contrary, a gradual decrease in the processing temperature to 250°C led to significant strengthening. The properties of bar processed under these conditions are as follows: UTS~430 MPa and YS~255 MPa and El~15% and close to ones usually obtained for this alloy after a full cycle of heat treatment, including quenching and aging. The mechanical properties obtained are comparable to ones obtained at different SPD methods.

Declarations

Funding: The research was supported by Russian Science Foundation (project No. 19-79-00054).

Competing interests: The authors have no competing interests to declare that are relevant to the content of this article.

Availability of data and material: The data that support the findings of this study are available from the corresponding author, A. Koshmin, upon reasonable request.

Code availability: Not applicable.

Ethics approval: Not applicable.

Consent to participate: Not applicable.

Consent for publication: All authors have read and agreed to the published version of the manuscript.

Authors' contributions: Conceptualization: Yury Gamin, Torgom Akopyan; Methodology: Sergey Galkin; Formal analysis and investigation: Alexander Koshmin, Vladimir Cheverikin, Tatiana Kin; Writing - original draft preparation: Yury Gamin, Tatiana Kin, Torgom Akopyan; Writing - review and editing: Sergey Galkin, Yury Gamin; Funding acquisition: Yury Gamin, Alexander Koshmin; Resources: Alexander Aleshchenko; Supervision: Sergey Galkin, Torgom Akopyan

References

1. Troeger LP, Starke EA (2000) Microstructural and mechanical characterization of a superplastic 6xxx aluminum alloy. Mater Sci Eng A. https://doi.org/10.1016/S0921-5093(99)00543-2
2. Heinz A, Haszler A, Keidel C, Moldenhauer S, Benedictus R, Miller WS (2000) Recent developments in aluminum alloys for aerospace applications. Mater Sci Eng A. https://doi.org/10.1016/S0921-5093(99)00674-7
3. Warner T (2006) Recently-Developed Aluminium Solutions for Aerospace Applications. MSF. https://doi.org/10.4028/www.scientific.net/msf.519-521.1271
4. Totten GE, MacKenzie DS (2003) Handbook of aluminium. Vol. 1. Physical metallurgy and processes. Marcel Dekker Inc, New York.
5. Dovzhenko, NN, Rushchits, SV, Dovzhenko, IN, Sidelnikov SB, Voroshilov DS, Demchenko AI, Baranov VN, Bezrukikh AI, Yuryev PO (2021) Deformation behavior during hot processing of the alloy of the Al-Mg system economically doped with scandium. Int J Adv Manuf Technol. https://doi.org/10.1007/s00170-021-07338-2
6. Yashin VV, Ruschits SV, Aryshensky EV, Latushkin IA (2019) Rheological behavior of 01570 and AA5182 wrought aluminum alloys under hot deformation conditions. Tsvetnye Metally. https://doi.org/10.17580/tsm.2019.03.09
7. Chen S-R, Wu C-Y, Yeh Y-L, Ou Y-L (2015) Hot deformation resistance of an AA5083 alloy under high strain rates. Key Eng Mater. https://doi.org/10.4028/www.scientific.net/KEM.626.553
8. Zhang X Y, Wang R, Wang XG (2021) Research on Hot Deformation Behaviors of 6061 Al Alloy. MSF. https://doi.org/10.4028/www.scientific.net/msf.1032.141
9. Gamin Y, Akopyan T, Koshmin A, Dolbachev A, Aleshchenko A, Galkin SP, Romantsev BA (2020) Investigation of the microstructure evolution and properties of A1050 aluminum alloy during radial-shear rolling using FEM analysis. Int J Adv Manuf Technol. https://doi.org/10.1007/s00170-020-05227-8
10. McQueen HJ (2004) Development of dynamic recrystallization theory. Mater Sci Eng A. https://doi.org/10.1016/j.msea.2004.01.064
11. Hallberg H, Wallin M, Ristinmaa M (2010) Modeling of continuous dynamic recrystallization in commercial-purity aluminum. Mater Sci Eng A. https://doi.org/10.1016/j.msea.2009.09.043

12. Hallberg H (2011) Approaches to Modeling of Recrystallization. Metals. https://doi.org/10.3390/met1010016
13. Gourdet S, Montheillet F (2003) A model of continuous dynamic recrystallization. Acta Materialia. https://doi.org/10.1016/S1359-6454(03)00078-8
14. Gourdet S, Montheillet F (2000) An experimental study of the recrystallization mechanism during hot deformation of aluminium. Mater Sci Eng A. https://doi.org/10.1016/S0921-5093(00)00733-4
15. Sellars CM, Zhu Q (2000) Microstructural modelling of aluminium alloys during thermomechanical processing. Mater Sci Eng A. https://doi.org/10.1016/S0921-5093(99)00648-6
16. Huang K, Logé RE (2016) A review of dynamic recrystallization phenomena in metallic materials. Mater Des. https://doi.org/10.1016/j.matdes.2016.09.012
17. Poliak EI (2020) Dynamic recrystallization control in hot rolling. Procedia Manuf. https://doi.org/10.1016/j.promfg.2020.08.067
18. Romantsev BA, Galkin SP, Mikhajlov VK, Khloponin VN, Koryshev AN (1995) Bar micromill. Steel Transl 2:40-42.
19. Galkin SP (2004) Regulating radial-shear and screw rolling on the basis of the metal trajectory. Steel Transl 34:57-60.
20. Naizabekov AB, Lezhnev SN, Panin E (2021) Formation of a Gradient Structure in Austenitic Stainless Steel AISI 321 by Radial-Shear Rolling. Solid State Phenom. https://doi.org/10.4028/www.scientific.net/ssp.316.246
21. Galkin SP, Romantsev BA, Kharitonov EA (2014) Putting into practice innovative potential in the universal radial-shear rolling process. CIS Iron Steel Rev 9:35-39.
22. Stefanik A, Szota P, Mróz S, Bajor T, Dyja H (2015) Properties of the AZ31 magnesium alloy round bars obtained in different rolling processes. Arch Metall Mater. https://doi.org/10.1515/amm-2015-0479
23. Thermo-Calc Software. ThermoTech Ltd. Databases. https://thermocalc.com/products/databases/thermotech-ltd-databases/. Accessed 24 Oct 2021.
24. Valiev R, Islamgaliev R, Alexandrov I (2000) Bulk nanostructured materials from severe plastic deformation. Prog Mater Sci. https://doi.org/10.1016/S0079-6425(99)00007-9
25. Valiev R, Estrin Y, Horita Z, Langdon T, Zechetbauer M, Zhu Y (2006) Producing bulk ultrafine-grained materials by severe plastic deformation. JOM. https://doi.org/10.1007/s11837-006-0213-7
26. Gamin YuV, Koshmin AN, Kin TYu, Aleshchenko AS (2021) Comparative analysis of stress-strain state of bars from aluminum alloys A2024 and A7075 processed by RSR based on FEM modeling. Mater Today: Proc.https://doi.org/10.1016/j.matpr.2021.03.106
27. Gamin Y, Koshmin A, Ta X (2020) Analysis of radial-shear rolling process parameters of aluminum alloys based on FEM modeling. MATEC Web Conf. https://doi.org/10.1051/matecconf/202031511001

28. Glazoff MV, Khvan AV, Zolotorevsky VS, Belov NA, Dinsdale AT (2019) Casting Aluminum Alloys. Their Physical and Mechanical Metallurgy. Elsevier,
29. Akopyan TK, Gamin YV, Galkin SP, Prosviryakov AS, Aleshchenko AS, Noshin MA, Koshmin AN, Fomin AV (2020) Radial-shear rolling of high-strength aluminum alloys: Finite element simulation and analysis of microstructure and mechanical properties. Mater Sci Eng A. https://doi.org/10.1016/j.msea.2020.139424
30. Akopyan TK, Belov NA, Aleshchenko AS, Galkin SP, Gamin YV, Gorshenkov MV, Cheverikin VV, Shurkin PK (2019) Formation of the gradient microstructure of a new Al alloy based on the Al-Zn-Mg-Fe-Ni system processed by radial-shear rolling. Mater Sci Eng A. https://doi.org/10.1016/j.msea.2019.01.029
31. Nikulin I, Malopheyev S, Kipelova A, Kaibyshev R (2012) Effect of SPD and friction stir welding on microstructure and mechanical properties of Al–Cu–Mg–Ag sheets. Mater Lett. https://doi.org/10.1016/j.matlet.2011.08.104.
32. Khafizova E, Islamgaliev R, Sitdikov V (2017) Strength and fatigue of an ultrafine-grained Al-Cu-Mg alloy. MATEC Web Conf. https://doi.org/10.1051/matecconf/201712902039

Figures

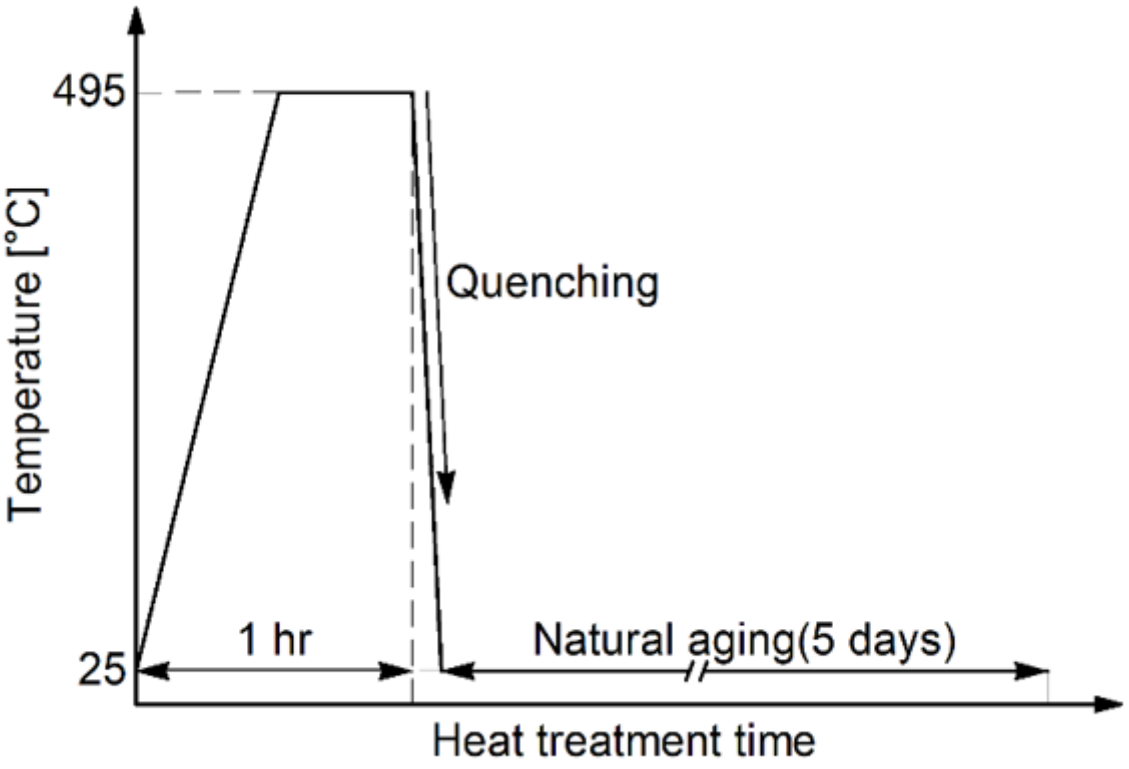

Figure 1

Heat treatment diagram

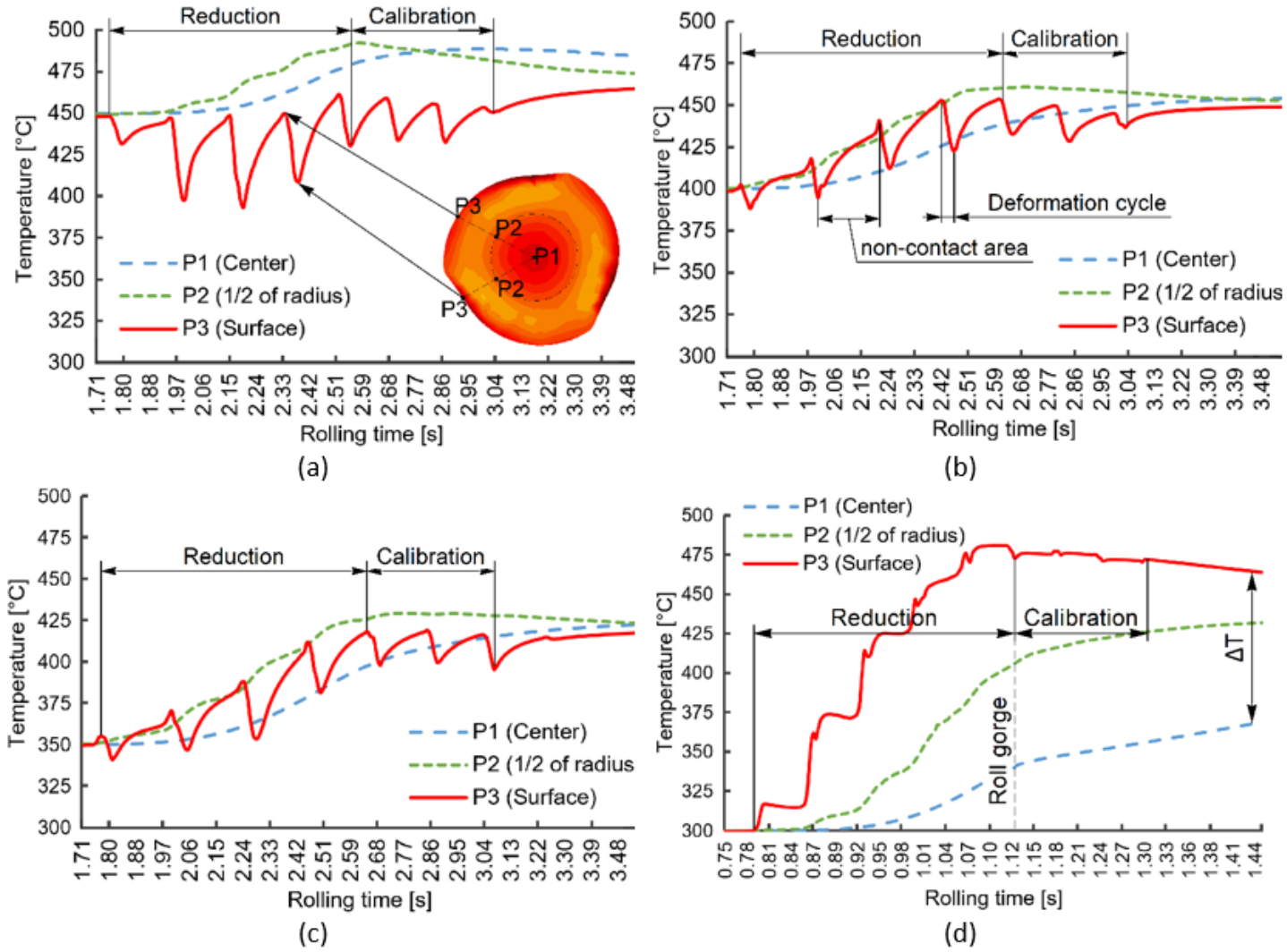

Figure 2

Temperature in deformation zone during 1st pass: (a) T0=450 °C, n=30 rpm; (b) T0=400 °C, n=30 rpm; (c) T0=350 °C, n=30 rpm; (d) T0=300 °C, n=90 rpm

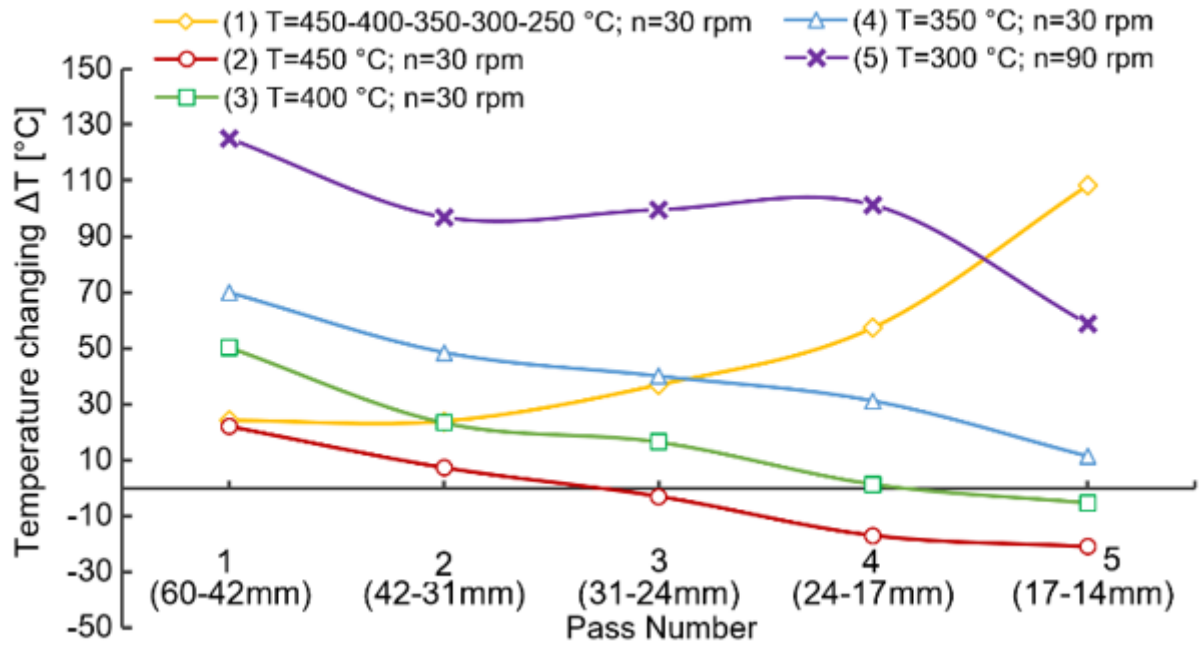

Figure 3

Average bar temperature change after each pass

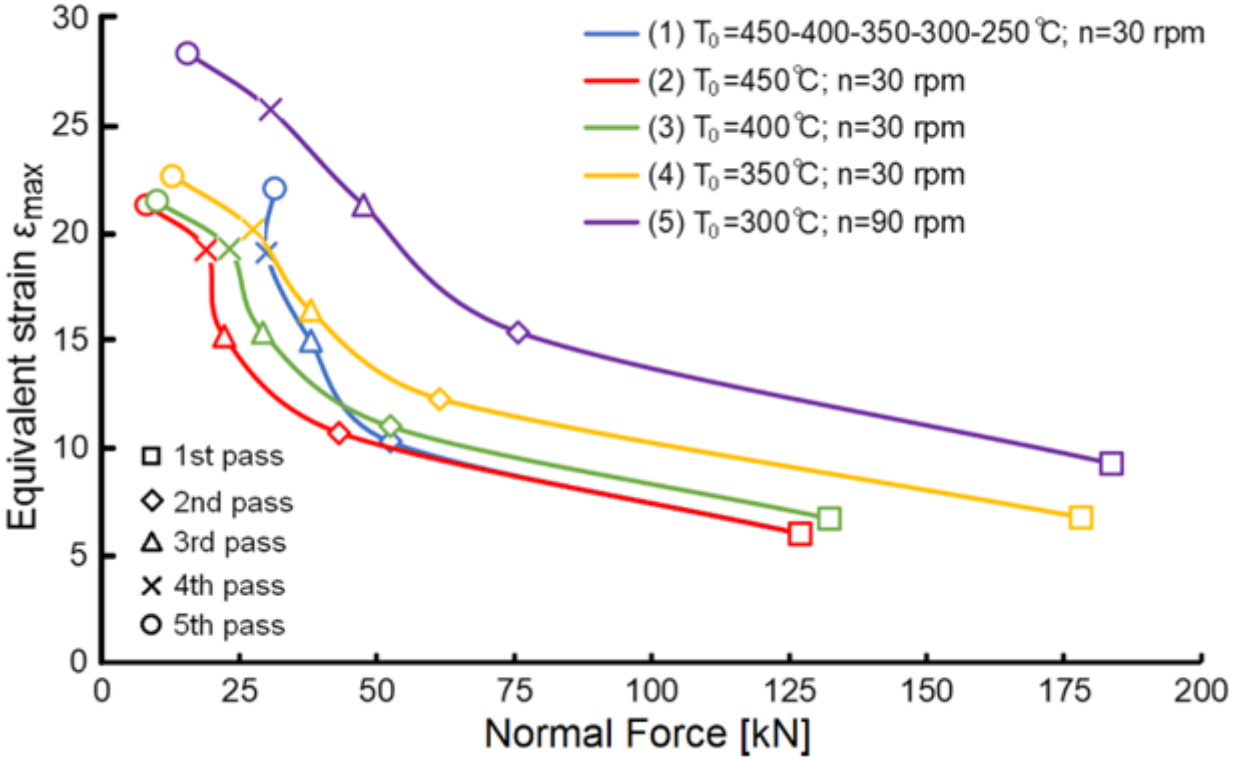

Figure 4

Dependence graphs of equivalent strain on workpiece surface (εmax) on the normal metal force on roll P in each pass

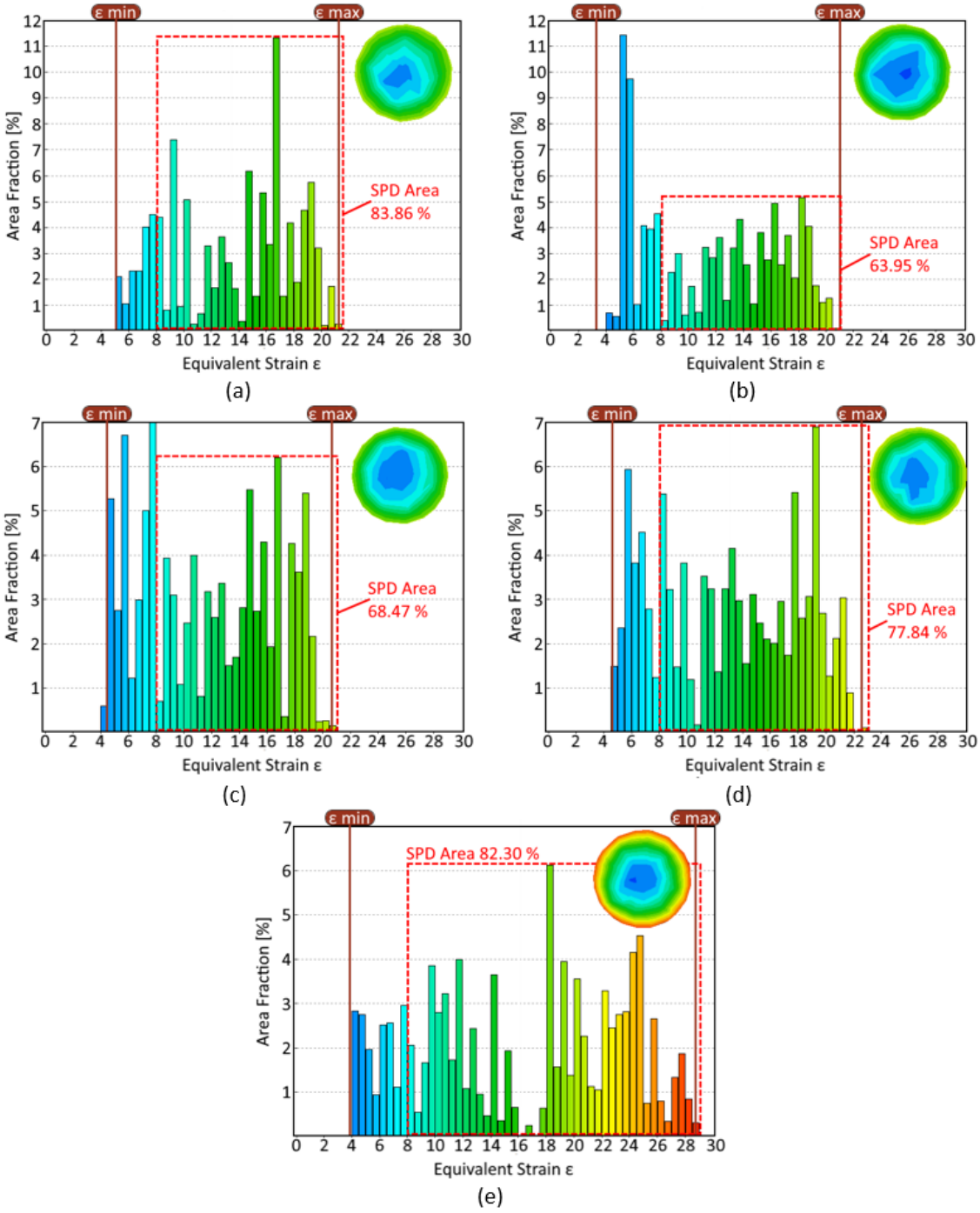

Figure 5

Equivalent strain distribution diagrams in the last pass (a) for regime 1; (b) regime 2; (c) regime 3; (d) regime 4; (e) regime 5

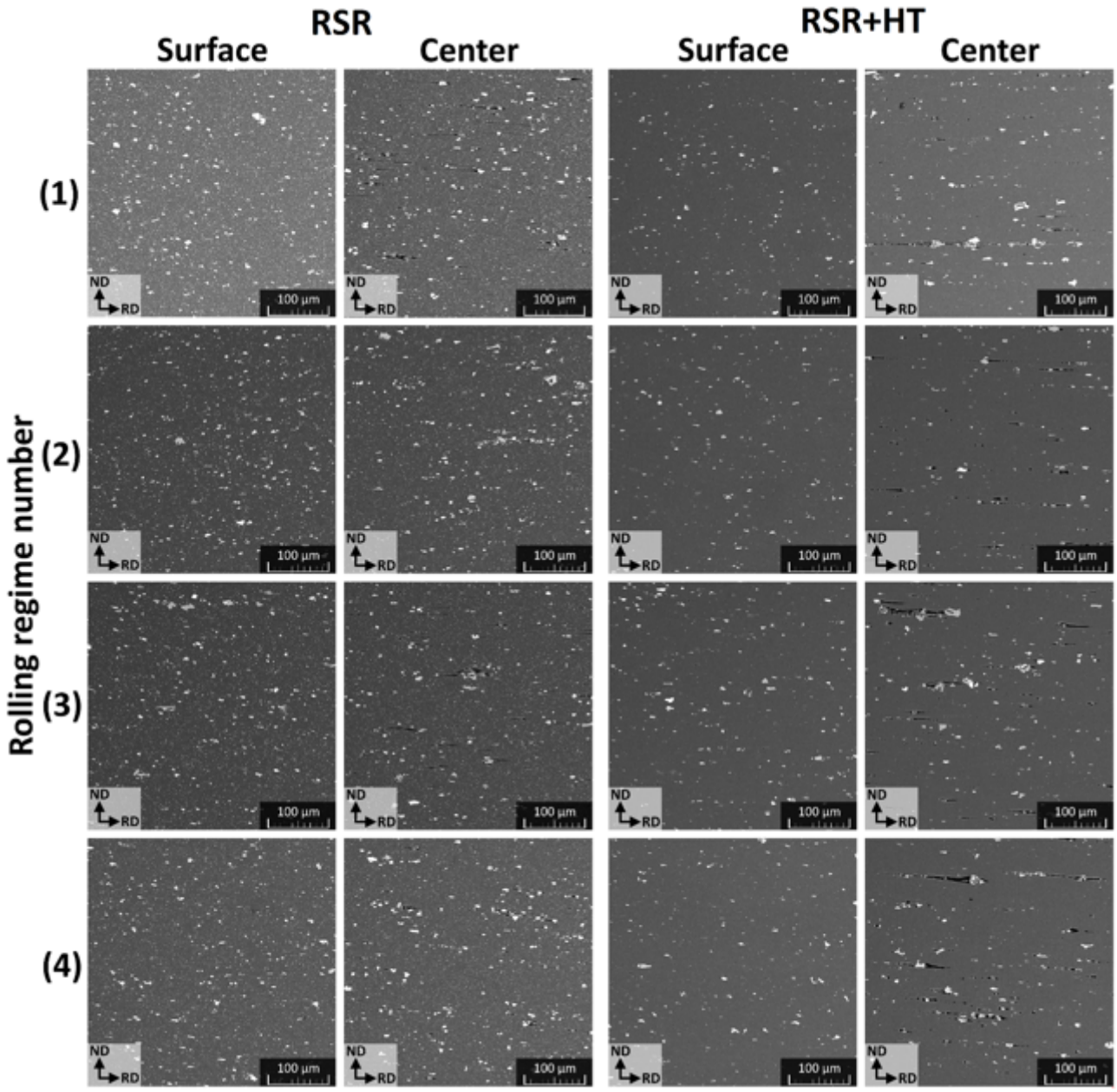

Figure 6

Microstructure (SEM) of A2024 alloy bars after RSR and after HT

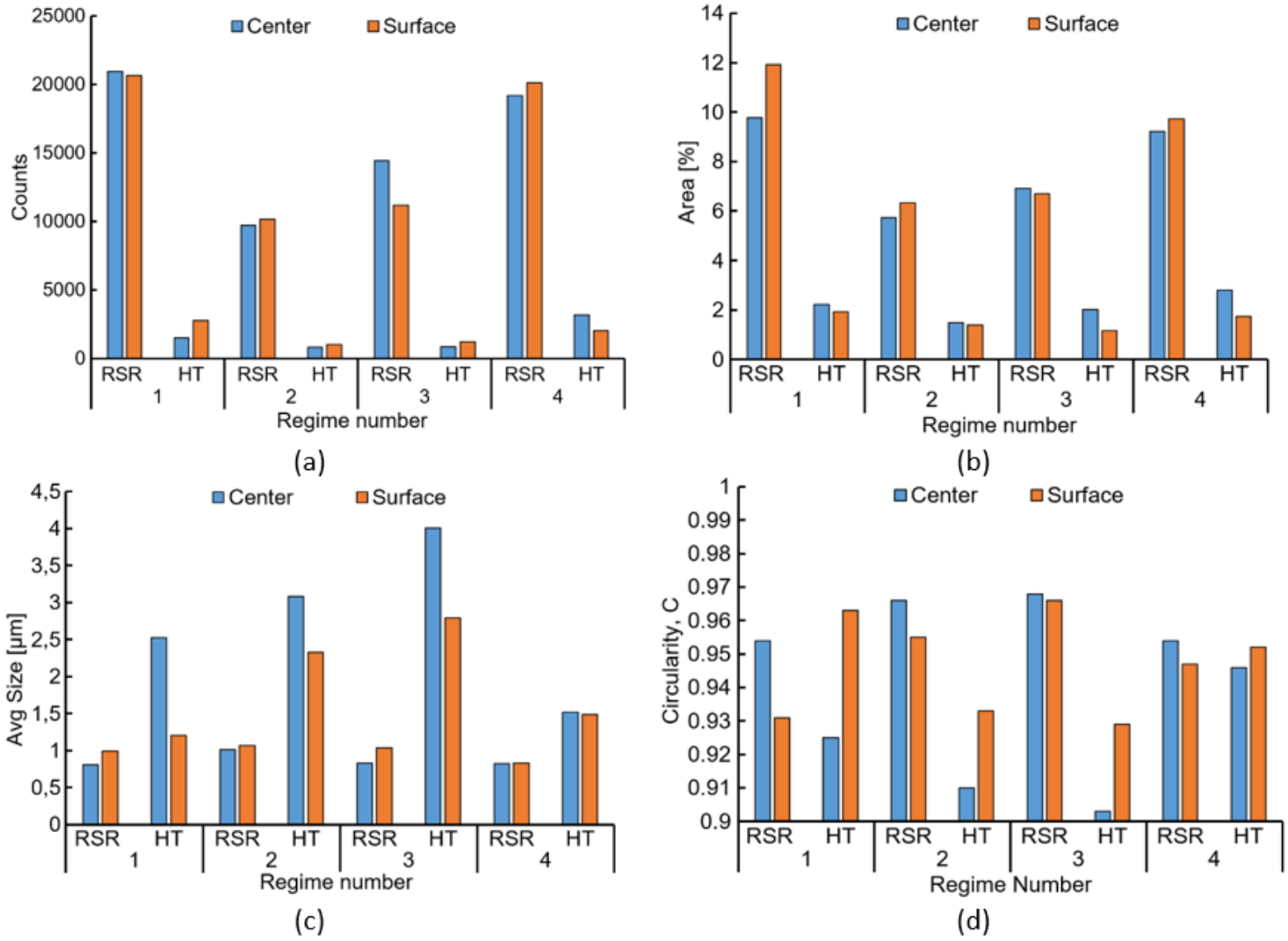

Figure 7

Diagrams of number (a), area (b), average size (c), and circularity (d) of secondary phases particles in A2024 alloys after RSR and HT

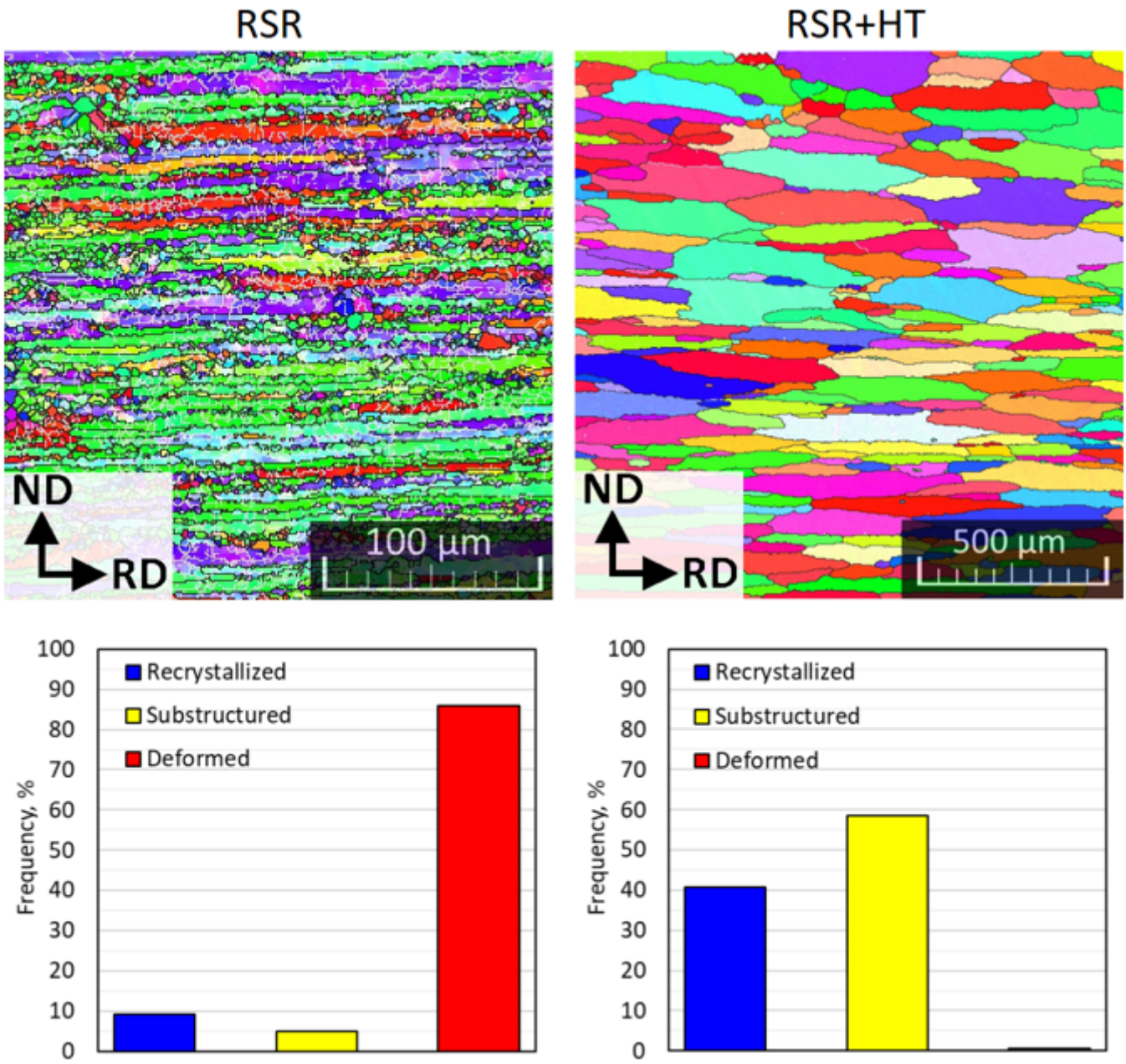

Figure 8

EBSD micrograph (color map) of grain orientation at the near surface of finished bar of 14 mm diameter obtained at rolling regime (1) and recrystallized, substructured and deformed fraction; (b, d) after RSR followed by annealing at 495 °C for 1 h. (For interpretation of the references to color in this figure legend, the reader is referred to the Web version of this article.)

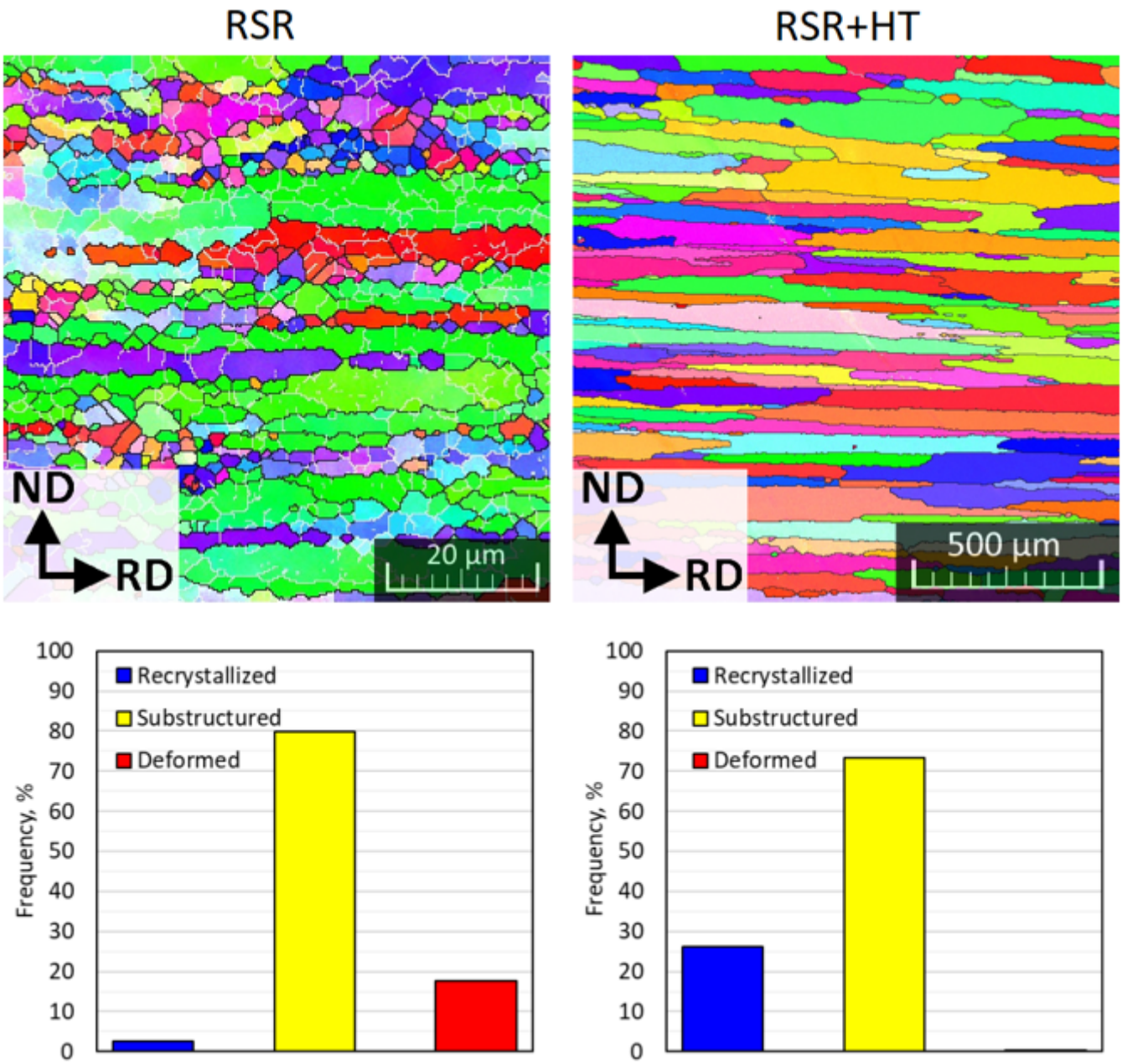

Figure 9

EBSD micrograph (color map) of grain orientation at the center of finished bar of 14 mm diameter obtained at rolling regime (1) and recrystallized, substructured and deformed fraction; (b, d) after RSR followed by annealing at 495 °C for 1 h. (For interpretation of the references to color in this figure legend, the reader is referred to the Web version of this article.)

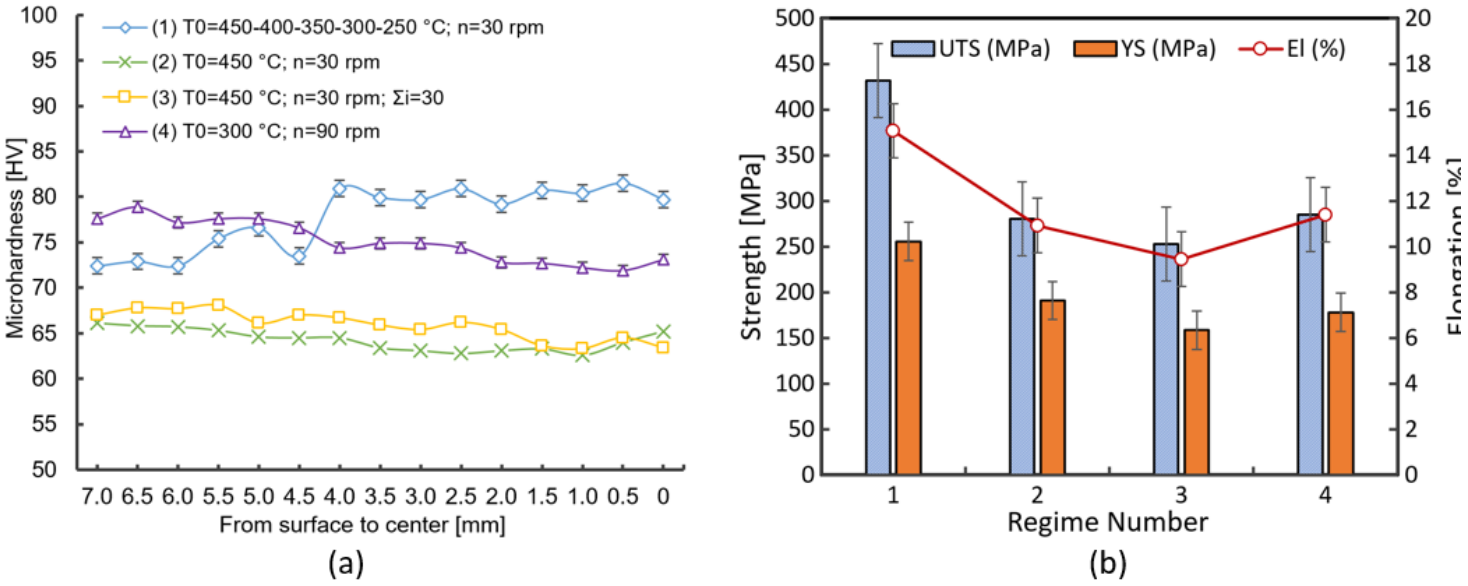

Figure 10

Microhardness distribution (a) and mechanical properties (b) of 14 mm as-processed bars